European Journal of Medicinal Chemistry 177 (2019) 221–234

Contents lists available at ScienceDirect

European Journal of Medicinal Chemistry

journal homepage: http://www.elsevier.com/locate/ejmech

Research paper

Dipropargyl substituted diphenylpyrimidines as dual inhibitors of monoamine oxidase and acetylcholinesterase

Bhupinder Kumar [a], Vijay Kumar [a], Vikash Prashar [b], Suresh Saini [a], Ashish Ranjan Dwivedi [a], Beenu Bajaj [a], Devashish Mehta [a], Jyoti Parkash [b, **], Vinod Kumar [a, *]

[a] Laboratory of Organic and Medicinal Chemistry, Department of Pharmaceutical Sciences and Natural Products, Central University of Punjab, Bathinda, Punjab, 151001, India
[b] Department of Animal Sciences, School of Basic and Applied Sciences, Central University of Punjab, Bathinda, Punjab, India

ARTICLE INFO

Article history:
Received 5 February 2019
Received in revised form
24 April 2019
Accepted 13 May 2019
Available online 16 May 2019

Keywords:
Alzheimer's disease
MAO inhibitors
Acetylcholinesterase inhibitors
Diphenylpyrimidine
Dual inhibitors
Neurological disorders

ABSTRACT

Alzheimer's disease (AD) is a multifactorial neurological disorder involving complex pathogenesis. Single target directed drugs proved ineffective and since last few years' different pharmacological strategies including multi-targeting agents are being explored for the effective drug development for AD. A total of 19 dipropargyl substituted diphenylpyrimidines have been synthesized and evaluated for the monoamine oxidase (MAO) and acetylcholinesterase (AChE) inhibition potential. All the compounds were found to be selective and reversible inhibitors of MAO-B isoform. These compounds also displayed good AChE inhibition potential with IC_{50} values in low micromolar range. **AVB4** was found to be the most potent MAO-B inhibitor with IC_{50} value of $1.49 \pm 0.09\ \mu M$ and **AVB1** was found to be the most potent AChE inhibitor with IC_{50} value of $1.35 \pm 0.03\ \mu M$. In the ROS protection inhibition studies, **AVB1** and **AVB4** displayed weak but interesting activity in SH-SY5Y cells. In the cytotoxicity studies involving SH-SY5Y cells, both **AVB1** and **AVB4** were found to be non-toxic to the tissue cells. In the molecular dynamic simulation studies of **30 ns,** the potent compounds were found to be quite stable in the active site of MAO-B and AChE. The results suggested that **AVB1** and **AVB4** are promising dual inhibitors and have the potential to be developed as anti-Alzheimer's drug.

1. Introduction

Alzheimer's disease (AD) [1] is a multifactorial neurological disorder characterized by memory loss and cognitive impairment. Pathophysiology of AD is highly complex and the disease state is associated with number of factors such as over expressed monoamine oxidase enzyme, declined levels of acetylcholine (ACh), hyperphosphorylation of tau proteins, amyloid-β aggregation and oxidative stress [2]. Neurodegeneration in AD causes neuronal and synaptic impairment which alters the concentration of various neurotransmitter systems in the brain that include cholinergic systems [3,4], dopamine, serotonin [5] and glutamate [2]. Thus, multi targeting agents (MTA) that can simultaneously modulate different cellular pathways are being explored as drug candidates to achieve better therapeutic efficacy for AD.

Monoamine oxidase (MAO) enzyme is considered as an important target for the treatment of AD [6]. It is involved in the oxidation of xenobiotic and endogenous monoamines including monoamine neurotransmitters such as serotonin, adrenaline, noradrenaline and dopamine. The oxidation reaction results in the formation of neurotoxic aldehydes and reactive oxygen species (ROS) as end products [7]. MAO enzyme exists in two different isoforms, MAO-A and MAO-B which differ in substrate and inhibitor specificity. MAO inhibitors have the potential to attenuate the oxidative metabolism of monoamine neurotransmitters and improve their concentration in the brain. MAO-A selective inhibitors are found to be effective

Abbreviations: QPlogBB, qualitatively predicted logarithmic ratio between the concentration of a compound in brain and blood; LogP, partition coefficient of a molecule between an aqueous and lipophilic phase (octanol and water); CAS, Catalytic active site; PAS, Peripheral active site; MTT, 3-(4,5-dimethylthiazol-2-yl)-2,5-diphenyltetrazolium; 6-OHDA, 6-hydroxydopamine; DMEM, Dulbecco's Modified Eagle's medium; HEPES, (4-(2-hydroxyethyl)-1-piperazineethanesulfonic acid).

* Corresponding author.
** Corresponding author.
E-mail addresses: Jyoti.parkash@cup.edu.in (J. Parkash), vpathania18@gmail.com, vinod.kumar@cup.ac.in (V. Kumar).

https://doi.org/10.1016/j.ejmech.2019.05.039
0223-5234/

against depression [8] while MAO-B selective inhibitors are being explored for the treatment of Parkinson's disease [9] and AD [10]. Recent studies have demonstrated that MAO-B inhibitors possess broader therapeutic effects such as neuroprotection [11], neurorescue [12] and cognitive improvement [7] which are useful for the treatment of AD.

Acetylcholine (ACh) is a neurotransmitter associated with cognitive functions and physical awareness [13]. ACh is hydrolyzed by acetylcholine esterase (AChE) or butyrylcholinesterase (BuChE) enzymes and imbalance in the dynamics is linked to the pathology of AD. The concentration of ACh is found to be drastically low in the AD patients as compared to the healthy persons. The peripheral anionic site (PAS) of AChE catalyzes amyloid-β aggregation which leads to the formation of senile plaques in the brain causing neurodegeneration [14]. Thus, AChE inhibitors can increase the cholinergic transmission in the synaptic cleft by inhibiting the degradation of ACh. At present donepezil, galantamine, and rivastigmine are three AChE inhibitors (Fig. 1) in the clinical practice for the treatment of AD [15]. These cholinergic drugs are able to provide symptomatic relief but could not prevent the progression of disease. Hence, using a single drug that act on a specific target may not be an efficient therapeutic strategy for AD due to its complex etiology. Now the attention of many research groups is focused on the multi-targeting agents (MTAs) to develop effective drug candidates for the treatment of AD. MTAs have the ability to bind to two or more targets and intervene in the pathological events underlying the etiology of the disease. The design strategy for MTA involves incorporation of pharmacophoric groups of different drugs in the same scaffold. Thus, a ligand with MAO inhibitory potential can exhibit more efficient therapeutic effect in AD when it can show additional AChE inhibitory activity. Consequently, many MTAs have been developed and some of them are in various stages of clinical development. Ladostigil (Fig. 1), a dual inhibitor of acetylcholinesterase and MAO-B, has completed phase II trial for AD (NCT01354691). Rasagiline (Fig. 1), is under phase-II clinical trials to determine its effect in the regional brain metabolism in case of AD (NCT02359552, NCT00104273).

In our previous studies [15], we have developed novel pyrimidine derivatives as selective inhibitors of MAO-B isoform. Most of these compounds were found to be reversible MAO-B inhibitors and taking leads from this study, we have developed another series of 4,6-diphenylpyrimidines as dual inhibitors of monoamine oxidase and acetylcholinesterase enzymes. In both of the studies, propargyl group was incorporated in the main scaffold as potential pharmacophore for MAO enzyme. Propargyl group is present in number of potent MAO inhibitors [10,16] such as clorgyline, selegiline, pargyline, rasagiline etc. and other multitargeting agents [17–25]. It forms a crucial covalent bond with the FAD cofactor of MAO enzyme [26]. Recently, Zindo et al. thoroughly reviewed the role of propargyl group as functional moiety in the design and development of multifunctional drugs for various neurological disorders [25]. Weinreb et al. [27] investigated the role of propargyl group in rasagiline as a neuroprotective moiety. It has been concluded that neuroprotective effect of rasagiline is associated with the propargyl moiety, which promotes mitochondrial viability and stabilizes permeability transition by regulating Bcl-2 family proteins. Similarly, other research groups [28,29] also demonstrated that rasagiline and other propargyl containing ligands may rescue degenerating dopamine neurons by inhibiting death signal transduction initiated by mitochondrial permeability transition. Keeping in view the significance of propargyl moiety and following our previous work, in the current study we have incorporated two propargyl groups in the diphenylpyrimidine scaffold and investigated their MAO and AChE inhibition potential. To the best of our knowledge this is first report on the screening of compounds containing two propargyl groups on a scaffold. The synthesized compounds were screened against MAO-A and MAO-B isoforms and all the compounds were found to be selective and reversible inhibitors of MAO-B isoform. These compounds also displayed good AChE inhibition potential with IC_{50} values in low micro molar range. In the series, **AVB4** was found to be the most potent MAO-B inhibitor with IC_{50} value of 1.49 ± 0.09 μM and **AVB1** was found to be the most potent AChE inhibitor with IC_{50} value of 1.35 ± 0.03 μM. In the ROS protection inhibition studies, **AVB1** and **AVB4** displayed weak but interesting activity in SH-SY5Y human neuroblastoma cells. The most active compounds were also tested for neuroprotective potential in SH-SY5Y cells and showed moderate activity. In the cytotoxicity studies involving SH-SY5Y cells, both **AVB1** and **AVB4** were found to be non-toxic to the tissue cells.

2. Results and discussions

2.1. Chemistry

All the compounds were synthesized by following the reaction procedures described in Scheme 1. All the final products were characterized by ^{1}H NMR, ^{13}C NMR, ESI-MS and HRMS.

2.2. Biological results

2.2.1. hMAO and AChE inhibition studies

MAO and AChE inhibition potential of the synthesized

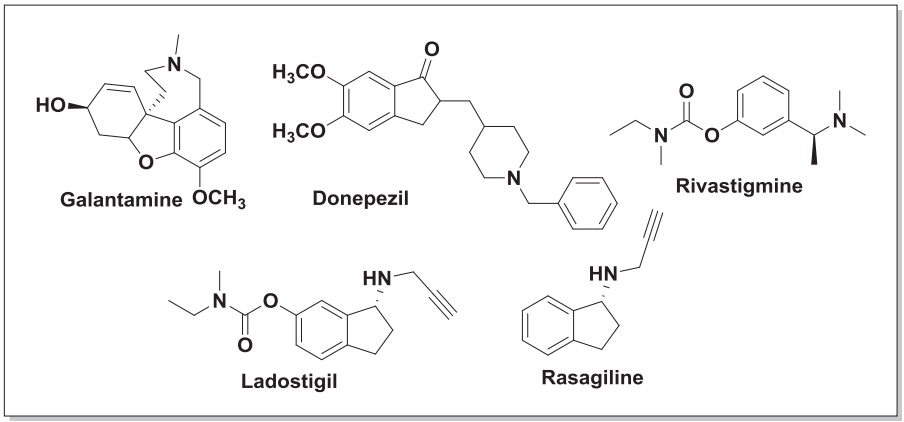

Fig. 1. Drugs in market and under clinical trials for Alzheimer's disease.

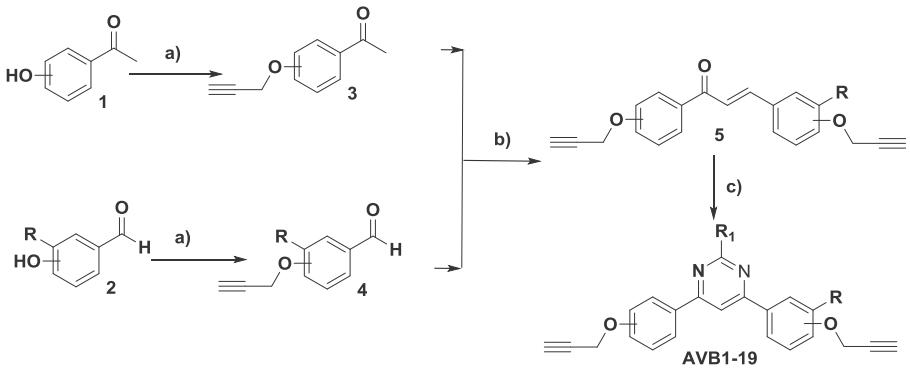

Scheme 1. Reagents and conditions: a) Propargyl bromide (1.2 eq), K_2CO_3 (2.4 eq), acetone, reflux, 12h; **b)** CH_3OH as solvent, 20% NaOH aq., rt, stirring 1h; **c)** Amidines (1.2 eq), Na_2CO_3 (2.4 eq), CH_3CN as solvent, reflux, 24h.

compounds (**AVB1**−**AVB19**) was evaluated through fluorimetric method using Amplex Red assay kits purchased from the Molecular Probes, Inc./Invitrogen. The results of MAO and AChE inhibition studies are expressed in the form of IC_{50} values (μM) described in Table 1. Both the phenyl rings of synthesized diphenylpyrimidine derivatives were substituted with propargyl groups at ortho/meta/para positions. Different amidines were used with R_1 as $-NH_2$, or $-CH_3$ or $-C_6H_5$ so as to develop structure activity relationship profile of this series of compounds. Clorgyline, pargyline, and donepezil were used as standard inhibitors for MAO-A, MAO-B, and AChE enzymes, respectively. All of the synthesized compounds were found to be potent inhibitors of MAO-B isoform (Selective over MAO-A) and AChE with IC_{50} values in low micromolar range. Compound **AVB4** was found to be the most potent MAO-B inhibitor with IC_{50} value of 1.49 ± 0.09 μM exhibiting 17-folds selectivity over MAO-A. It also showed potent inhibition of AChE with IC_{50} value of 1.74 ± 0.07 μM. In the reported series, **AVB1** was found to be the most potent AChE inhibitor with an IC_{50} value of 1.35 ± 0.03 μM and displayed MAO-B inhibitory activity with an IC_{50} value of 3.30 ± 1.17 μM. Unfortunately, as evident from Table 1, all the compounds were found to be unselective or weakly selective for MAO-B isoform.

2.2.2. Reversibility inhibition studies

To determine whether the synthesized compounds are reversible or irreversible inhibitors of the target enzymes, the most active

Table 1
Results of MAO-A, MAO-B and AChE inhibition studies of the synthesized compounds..

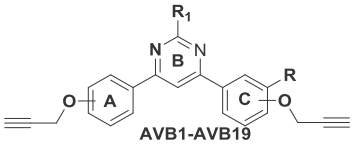

Entry Name	Propargyl at ring A	Propargyl at ring C	R	R_1	IC_{50} values (mean ± S.E. μM)			MAO Selectivity (SI)
					hMAO-A	hMAO-B	eeAChE	
AVB1	C4	C4	H	NH_2	32.06 ± 1.19	3.30 ± 1.17	1.35 ± 0.03	9.7
AVB2	C4	C4	H	CH_3	34.15 ± 2.03	7.83 ± 0.57	1.76 ± 0.06	4.4
AVB3	C4	C4	H	C_6H_5	25.57 ± 1.18	12.26 ± 0.99	7.53 ± 0.23	2.1
AVB4	C4	C3	H	NH_2	24.06 ± 0.71	1.49 ± 0.09	1.74 ± 0.07	16.1
AVB5	C4	C3	H	CH_3	21.14 ± 1.40	8.09 ± 0.54	5.88 ± 0.07	2.6
AVB6	C4	C3	H	C_6H_5	25.83 ± 1.92	17.69 ± 1.13	4.39 ± 0.16	1.5
AVB7	C4	C2	H	NH_2	28.55 ± 0.77	22.12 ± 1.68	1.81 ± 0.02	1.3
AVB8	C4	C2	H	CH_3	23.19 ± 1.87	18.07 ± 1.75	2.56 ± 0.13	1.3
AVB9	C4	C2	H	C_6H_5	22.02 ± 1.03	14.44 ± 0.78	7.25 ± 0.16	1.5
AVB10	C3	C3	H	NH_2	***	22.09 ± 0.94	6.99 ± 0.09	≥3
AVB11	C3	C3	H	C_6H_5	***	23.44 ± 1.17	6.73 ± 0.18	≥3
AVB12	C2	C2	H	NH_2	***	11.13 ± 0.16	5.19 ± 0.21	≥5
AVB13	C2	C2	H	C_6H_5	***	13.78 ± 0.22	8.12 ± 0.19	≥4
AVB14	C4	C4	OCH_3	NH_2	***	20.03 ± 1.18	4.58 ± 0.08	≥3
AVB15	C4	C4	OCH_3	CH_3	24.99 ± 2.13	21.08 ± 1.83	5.92 ± 0.18	1.2
AVB16	C4	C4	OCH_3	C_6H_5	24.93 ± 1.17	15.71 ± 0.95	6.99 ± 0.16	1.6
AVB17	C4	C4	OCH_2CH_3	NH_2	***	14.01 ± 1.07	7.05 ± 0.14	≥4
AVB18	C4	C4	OCH_2CH_3	CH_3	***	10.97 ± 0.82	6.38 ± 0.09	≥5
AVB19	C4	C4	OCH_2CH_3	C_6H_5	***	29.03 ± 1.33	6.94 ± 0.16	≥2
Clorgyline					4.39 ± 1.02 nM	nd	nd	
Pargyline					nd	0.15 ± 0.02	nd	
Donepezil					nd	nd	0.03 ± 0.001	

***Inactive or showed less than 50% inhibitory activity at 50 μM concentration and precipitated at higher concentrations. [nd]not determined, SI for MAO-B: IC_{50} MAO-A/IC_{50} MAO-B.

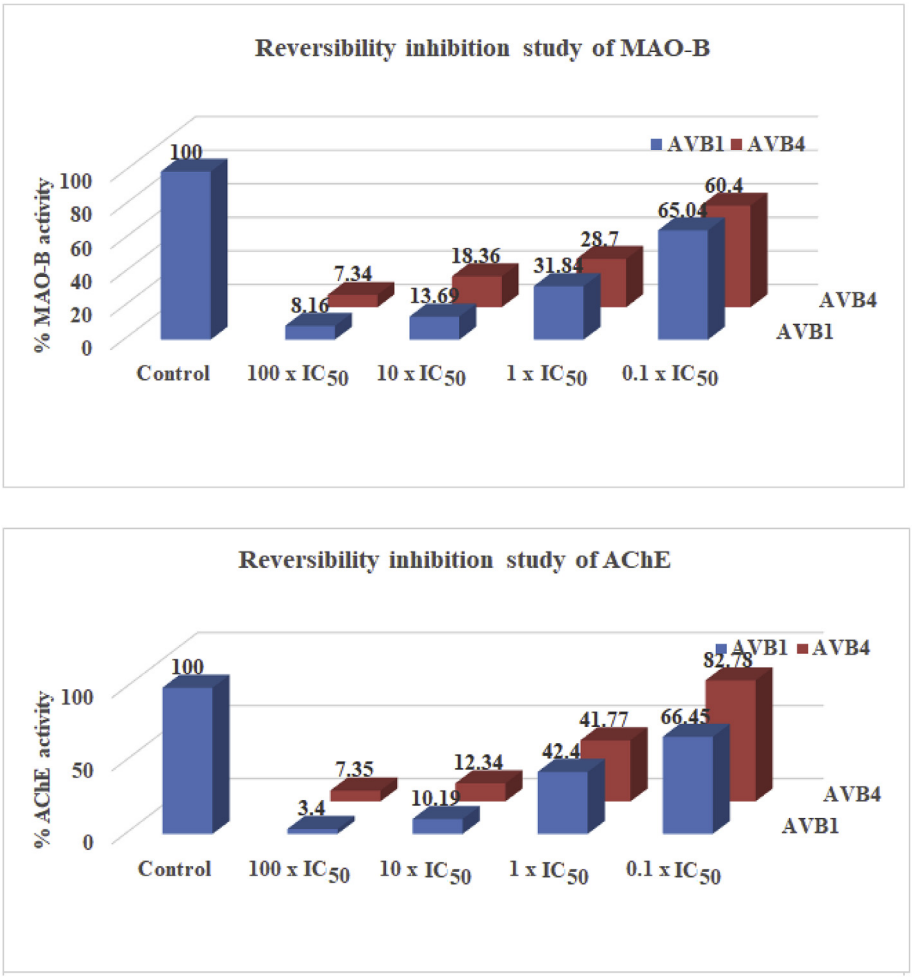

Fig. 2. Reversibility inhibition studies of **AVB1** and **AVB4** with **A)** MAO-B enzyme and **B)** AChE enzyme.

compounds i.e. **AVB1** and **AVB4** were subjected to reversibility inhibition studies [15]. Both the compounds were found to be reversible inhibitors of MAO-B and AChE enzymes. At the IC_{50} concentration **AVB1** showed 31.8% and 42.4% residual activity for MAO-B and AChE respectively. Similarly, **AVB4** displayed 28.7% and 41.7% residual activity for MAO-B and AChE respectively. Compound **AVB1** showed recovery in the enzyme activity by up to 65.04% and 66.45% for MAO-B and AChE respectively at 0.1 X IC_{50} concentration, while compound **AVB4** showed recovery in the enzyme activity up to 60.4% and 82.78% for MAO-B and AChE respectively at 0.1 X IC_{50} concentration (Fig. 2). At 1 X IC_{50} concentration of compound **AVB1**, enzymatic activity upto 31.84% and 42.4% was recovered for MAO-B and AChE respectively, while for **AVB4**, enzymatic activity upto 28.7% and 41.7% was recovered for MAO-B and AChE respectively. Thus, it can be concluded that the synthesized compounds are weak reversible inhibitors of both MAO-B and AChE enzymes at 1 X IC_{50} concentration of these inhibitors.

2.2.3. Kinetic studies of AChE inhibition

To determine the mechanism of inhibition of AChE, kinetic study was carried out with the most potent inhibitor of AChE (**AVB4**) using eeAChE. The reciprocal Lineweaver-Burk plots (Fig. 3) illustrates the increased slope (decreased V_{max}) and higher intercepts (K_m) with the increasing concentration of **AVB4.** The intersection point of the Lineweaver-Burk reciprocal plots was located in the third quadrant, which indicate that **AVB4** is mixed type inhibitor. **AVB4** might be binding to PAS and CAS of AChE simultaneously and inhibit the binding of substrate to active site. Binding of **AVB4** with the PAS and CAS is further supported by docking and molecular dynamics simulation studies.

2.2.4. ROS inhibition studies

From literature survey, it is clear that MAO mediated metabolism of various monoamines leads to the production of H_2O_2 which further get converted into free radicals through Fenton's reaction and induces oxidative stress. Increased levels of these free radicals, initiate free radical-mediated chain reactions that may cause oxidative damage to the cell membranes, DNA strand breakdown and neuronal cell death. Thus, prevention of ROS generation along with MAO inhibition is considered as an added advantage to prevent neurotoxicity in neurodegenerative diseases. The most potent compounds in the series i.e. **AVB1** and **AVB4** were evaluated for their ROS production inhibition potential against human neuroblastoma cells (SH-SY5Y) after 24h interval treatment. For activity evaluation, 2,7-dichlorofluorescein diacetate (DCF-DA), a non-fluorescent compound was used. DCF-DA in the presence of reactive oxygen species is oxidized to 2,7-DCF which is a fluorescence emitting agent. Compound **AVB1** reduced the ROS levels to 89.83% and 30.04% at 1 μM and 5 μM concentrations, respectively in the SH-SY5Y cells (Fig. 4). Similarly, compound **AVB4** reduced the ROS levels up to 68.3% and 47.25% at 1 μM and 5 μM concentrations,

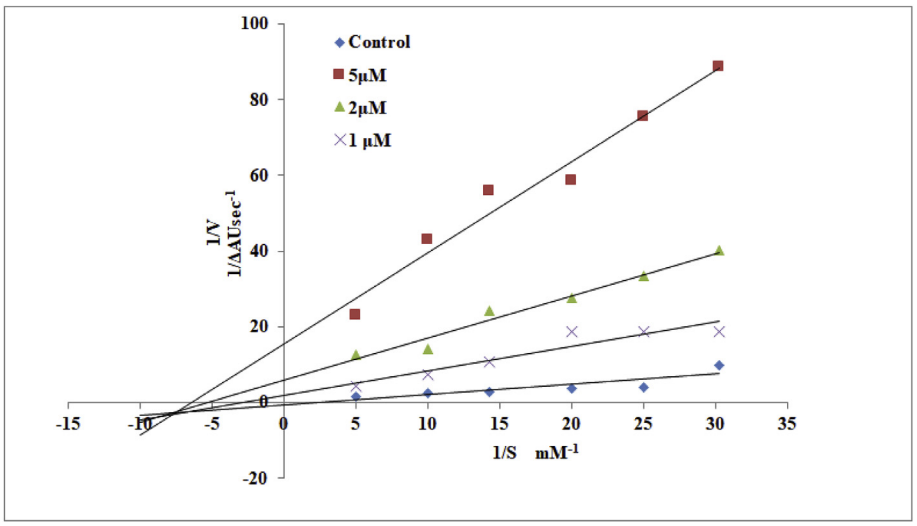

Fig. 3. Kinetic study on the mechanism of *ee*AChE inhibition by **AVB4**. Overlaid Lineweaver–Burk reciprocal plots of AChE initial velocity at increasing substrate concentration (0.1–1 mM) in the absence or presence of **AVB4** are shown.

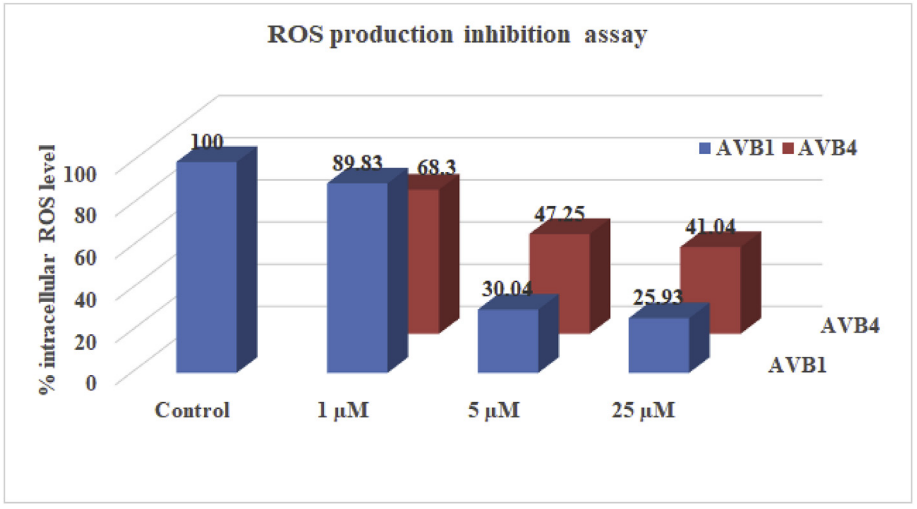

Fig. 4. ROS inhibition studies of compound **AVB1** and **AVB4** on SH-SY5Y cells after treatment for 24h.

respectively in the SH-SY5Y cells. Thus, from these results, it is apparent that this series of compounds with two propargyl moieties may weakly protect the neuronal cells from ROS.

2.2.5. Neuroprotective effects

The most potent AChE and MAO-B inhibitors i.e **AVB1** and **AVB4** were evaluated for their neuroprotective potential against 6-hydroxydopamine (6-OHDA) neurotoxin in SH-SY5Y cells. These compounds showed mild neuroprotective potential against 6-OHDA. Maximum cell viability of 66.6% was observed for compound **AVB1** as compared to the 6-OHDA treated cells (48.52%). As the concentration of the compounds increased from 5 μM to 25 μM, the cell viability was further reduced as shown in Fig. 5.

2.2.6. Metal chelation studies

Metal-chelating studies of **AVB1** and **AVB4** were performed with a UV–vis spectrophotometer. The absorption spectra of both compounds (50 μM, final concentration) alone or in the presence of $CuSO_4$, $FeSO_4$, and $FeCl_3$ (50 μM, final concentration) were recorded. In metal chelating studies, none of the compounds formed any metal chelate with any of the above metal salts. Thus, these compounds are ineffective against metal salts and did not show any metal chelating properties.

2.2.7. Cytotoxicity studies

Cytotoxicity of the most potent inhibitors (**AVB1 and AVB4**) was determined against SH-SY5Y cells using MTT assay. The test compounds at 1 μM, 5 μM and 25 μM concentrations were incubated with SH-SY5Y cells and cell viability was determined after 24h time interval using MTT assay. As depicted in Fig. 6, the compounds were found non-toxic at the lower concentrations. As the concentration of the compounds increased, there was a slight decrease in the cell viability. Minimum cell viability of 69.17% was observed for **AVB4** at 25 μM concentration. At lower concentration of 1 μM, cell viability of 87.34% was observed as compared to the control. Thus, keeping in view the IC_{50} values of the compounds which are in low

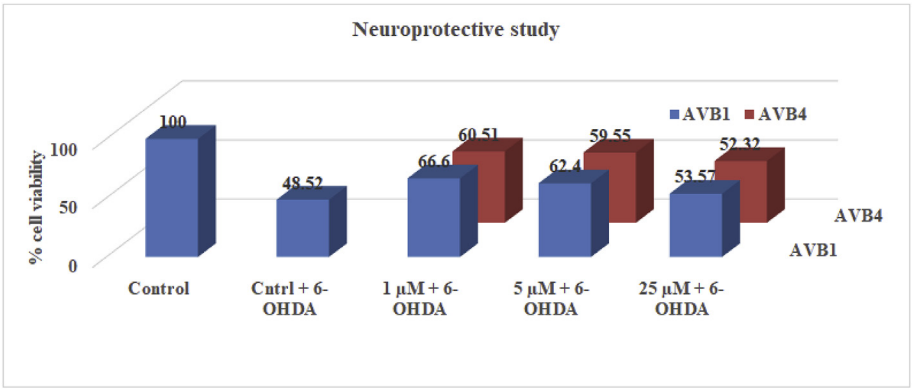

Fig. 5. Neuroprotective studies of **AVB1** and **AVB4** on SH-SY5Y cells.

micromolar range, the current series of compounds were found to be nontoxic to the tissue cells (Fig. 6).

2.2.8. *Molecular docking and simulation studies*

Docking of the ligands and molecular dynamics simulations in the active site of the receptors may provide crucial information about the orientations of the ligands and their interactions with various amino acid residues at the receptor site. Most active compounds obtained in the series were docked at the respective active sites of the receptor isoforms. Maestro 11.1 (Schrödinger LLC) software was used for carrying out the docking studies and compounds **AVB1** and **AVB4** were docked at the hMAO-B (PDB ID-2BYB) [30] and AChE (PDB ID-1EVE) [31] and their crystal structures were imported from the protein data bank. The docking procedures were first validated by accurately redocking the co-crystallized ligands into the MAO models. The active site of MAO-B is divided into two different compartments, an entrance cavity and a substrate cavity separated by the side chain of Ile199 which serves as a "gate" between the two cavities. The docking orientations of the compound **AVB1** and **AVB4** showed that the pyrimidine moiety in both the compounds interact with the Ile199 and kept this residue in open gate conformation. Phenyl ring with propargyl group at meta position in **AVB4** is oriented towards FAD cofactor and accommodated in the substrate cavity while the phenyl ring with para propargyl group is aligned in the entrance cavity. In the enzyme-AVB1 complex, both the phenyl rings contain propargyl groups at the para positions and one of the propargyl group is oriented towards the FAD cofactor. The NH_2 group of **AVB1** showed hydrogen bonding with Phe168 and Cys172. In the enzyme-AVB4 complex**,** pyrimidine ring remains close to the entrance cavity and NH_2 group formed hydrogen bonds with Cys172 and Tyr188. The pyrimidine ring in **AVB1** form π-π stacking with Tyr326 while in **AVB4** propargyl containing phenyl ring interacts with Tyr326 as shown in Fig. 7. The inner phenyl ring of **AVB4** in the substrate displayed π-π interactions with Phe343. The increased MAO-B activity of **AVB4** as compared to **AVB1** might be due to the additional π-π stacking of **AVB4** with Tyr326 and Phe343.

Similarly, both of these compounds i.e. **AVB1** and **AVB4** were docked against AChE (PDB ID- 1EVE co-crystallized with donepezil) to determine their binding alignment at the active site of the enzyme. The active site of AChE is divided into two compartments; i) catalytic active site (CAS) composed of Trp84, Tyr130, Phe330, Phe331 residues and, ii) peripheral anionic site (PAS) which consists of amino acids-Tyr70, Asp72, Tyr121, Trp279, and Tyr334. The compounds were found to interact both with CAS as well as with PAS of AChE. Pyrimidine ring in **AVB1** and **AVB4** accommodated in PAS and NH_2 group formed hydrogen bonds with Asp72 (Fig. 8). In case of **AVB1,** one of the phenyl rings with a propargyl group is accommodated in the CAS and showed π-π interactions with Trp84. In **AVB4,** phenyl ring with para propargyl group is oriented towards PAS and displayed π-π stacking with Tyr334. An additional hydrogen bond interaction of *O*-propargylated group with Phe288 in PAS was observed in **AVB1** (Fig. 8). Thus, interactions of these compounds at CAS, as well as PAS, make them more effective against AD.

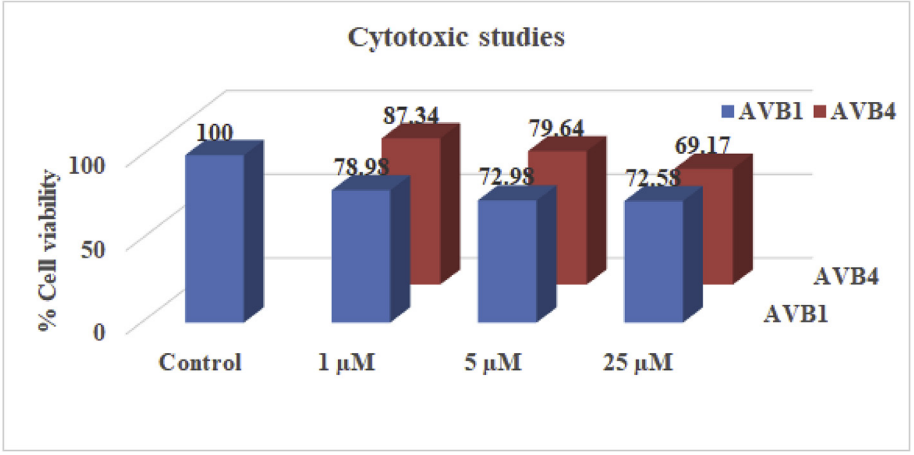

Fig. 6. Cytotoxicity studies of **AVB1** and **AVB4** on the SH-SY5Y cells after treatment for 24h.

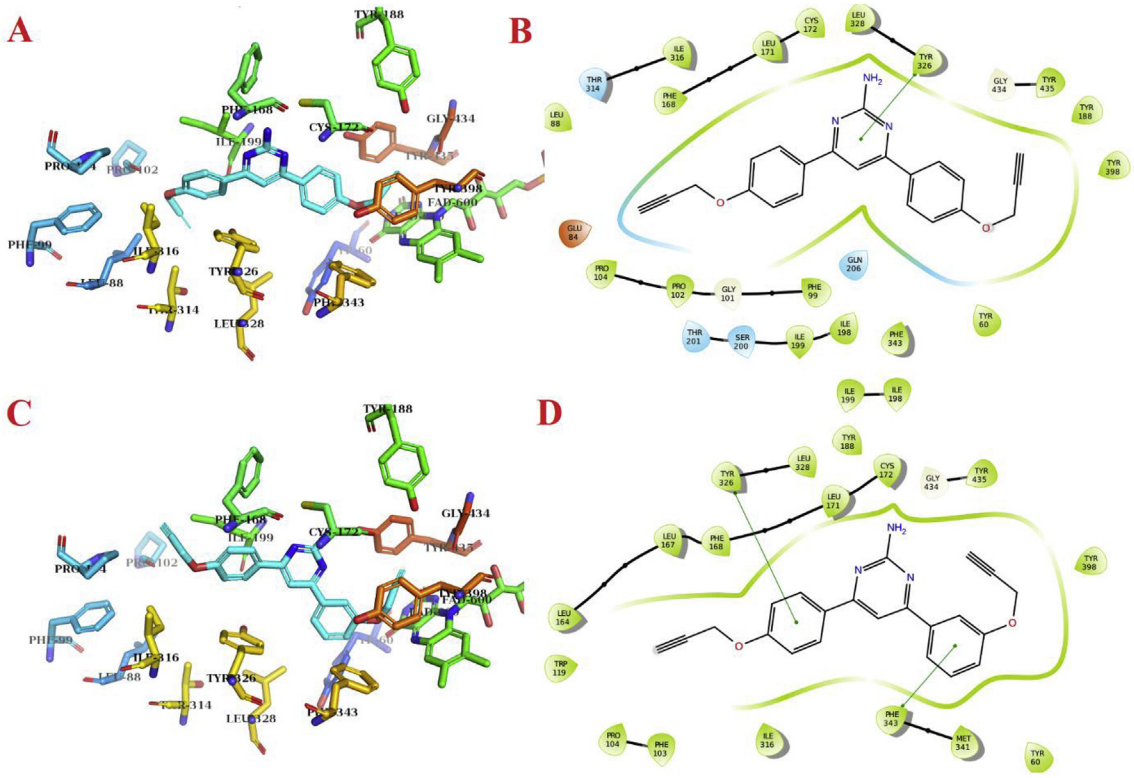

Fig. 7. A) Binding pattern (3D) of **AVB1** with the amino acid residues at the active site of MAO-B (2BYB), **B)** binding interactions (2D) of **AVB1** with various amino acids of MAO-B active cavity, **C**) Binding pattern (3D) of **AVB4** with the amino acid residues at the active site of MAO-B (2BYB), and **D)** binding interactions (2D) of **AVB4** with various amino acids of MAO-B active cavity.

2.2.9. Molecular dynamic simulation studies

In order to investigate the binding stability of the potent inhibitors into the active site of the MAO-B and AChE, molecular dynamic (MD) simulations studies were performed. For this docking complexes of **AVB1** and **AVB4** with MAO-B and AChE were used. The MD simulations studies were conducted for 30 ns and the interaction pattern of the test compounds with different amino acids was analyzed. MD simulations studies of **AVB4** with MAO-B yielded the stable trajectory from 3 ns to 30 ns, oscillating in between 0.8 Å to 1.2 Å. For the initial 2 ns time interval, a sharp hike was observed in RMSD from 0.4 Å to 1.6 Å, which stabilized to 1.2 Å after 3 ns interval. The pyrimidine ring of AVB4 maintained its initial ð-ð interaction with Tyr326 throughout MD time interval (Fig. 9).

Similarly, docking complexes of **AVB1** and **AVB4** with AChE were used for MD simulations to determine their binding stability at the active site of the enzyme. In case of **AVB4,** a stable trajectory was observed after the initial 3 ns interval which was determined through root-mean-square-deviation (RMSD) of the protein backbone ranging from 0.8 Å to 1.2 Å (Fig. 10). For the first 3 ns time interval, a hike in RMSD trajectory was observed from 0.4 Å to 0.8 Å. In case of **AVB1,** RMSD kept oscillating from 0.4 Å to 1.2 Å throughout the MD simulations studies of 30 ns. Analyzing these MD trajectories of AChE-AVB1 and AChE-AVB4 complexes, it can be concluded that these compounds (**AVB1** and **AVB4**) had a strong tendency to be localized in the binding region of AChE. One of the propargyl substituted ring of **AVB1** maintained its initial π-π interaction with Trp84. Similarly, for **AVB4** the initial interactions such as hydrogen bond formation of pyrimidine ring with Tyr121 and π-π interactions of pyrimidine ring with Trp84 were maintained throughout the MD simulations time interval (Fig. 10). Thus from these studies, it can be concluded that MD simulations of **AVB1** and **AVB4** do not indicate any abrupt local force that could potentially break up the inhibitors or can even delocalize these from the binding site of AChE.

2.2.9. Physicochemical properties

In order to assess the drug-like characteristics of the most active compounds (**AVB1** and **AVB4**), various physicochemical parameters of these compounds have been evaluated. Both the compounds showed good drug-like properties and follow Lipinski's rule of five (see Table 2). The logP value of both the compounds is less than five and hydrogen bond donor and acceptor atoms are also less than five. Both the compounds showed 100% human oral absorption in Qikprop studies. The QPlogBB values were also in the optimum range and hence these compounds are expected to cross the blood-brain barrier. Thus, it can be concluded that both of these compounds have an optimum chemical skeleton that can be developed as potential drug molecule.

2.2.10. SAR studies

In the current studies, diphenylpyrimidines containing two propargyl groups were designed and synthesized. A total of 19 compounds were synthesized and evaluated against MAO-A, MAO-B and AChE enzymes. Most of the compounds of this series were found to be selective inhibitors of MAO-B isoform and also displayed potent AChE inhibitory activities. As evident from Table 1, **AVB1** with propargyl groups at the para positions of the phenyl rings and a NH_2 group on the pyrimidine ring displayed IC_{50} values of 1.74 ± 0.07 μM and 1.35 ± 0.03 μM for MAO-B and AChE respectively. **AVB1** was found to be the most potent AChE inhibitor in the reported series of compounds. Replacement of NH_2 with CH_3 in **AVB2** reduced MAO-B inhibitory activity by more than 2-folds but

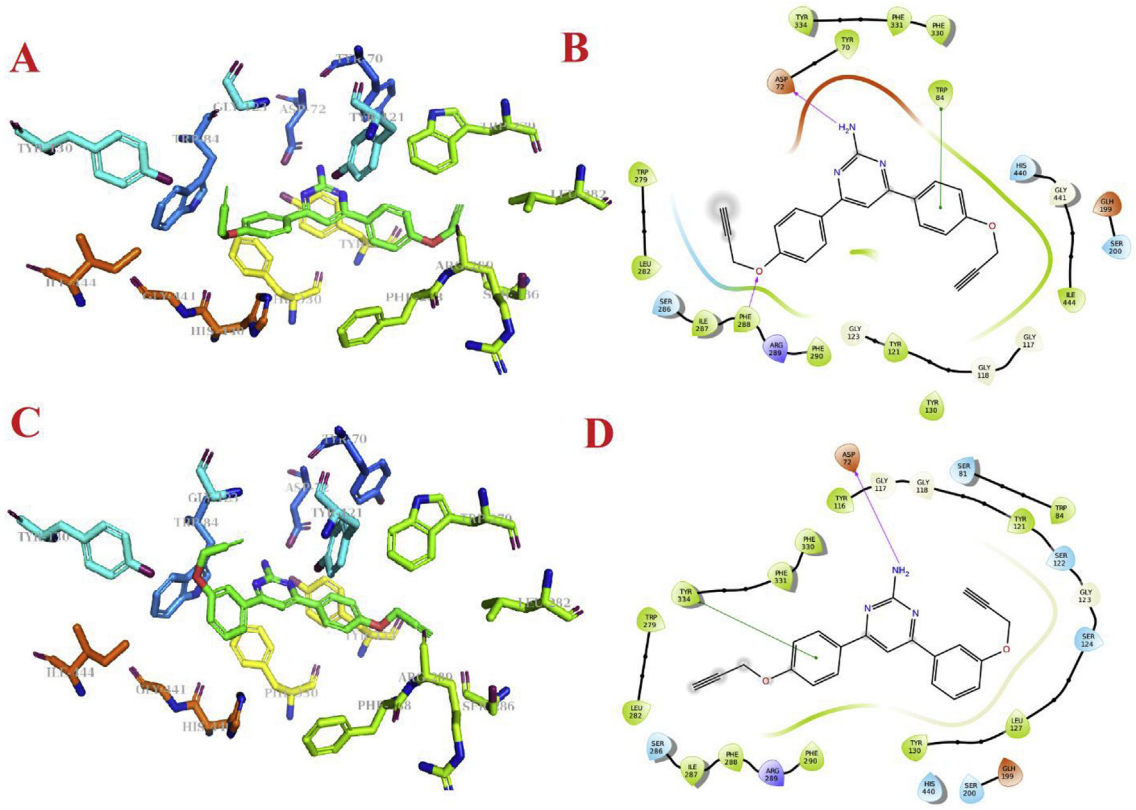

Fig. 8. A) Binding pattern (3D) of **AVB1** with the amino acid residues at the active site of AChE (1EVE)**, B)** binding interactions (2D) of **AVB1** with various amino acids of AChE active cavity, **C**) Binding pattern (3D) of **AVB4** with the amino acid residues at the active site of AChE (1EVE)**,** and **D)** binding interactions (2D) of **AVB4** with various amino acids of AChE active cavity.

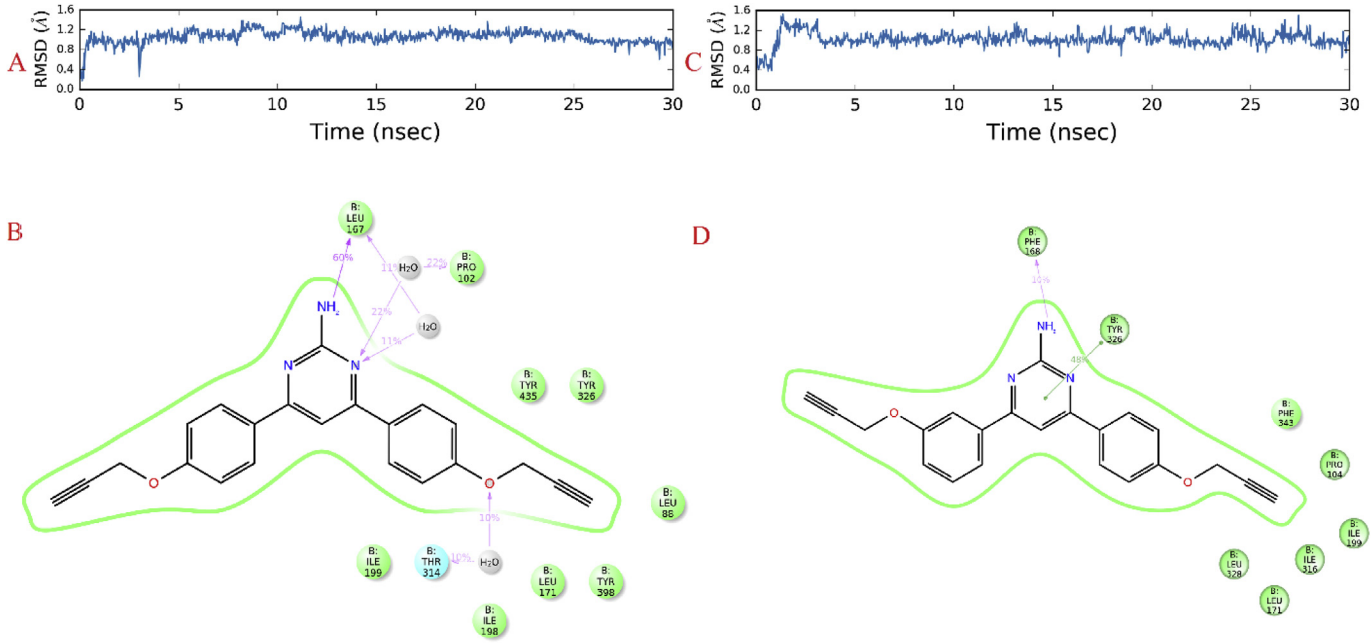

Fig. 9. A) RMSD graph of MD simulations studies of **AVB1** with MAO-B for 30 ns, **B**) interactions of **AVB1** with the active site residues of MAO-B during 30 ns MD simulations studies, **C)** RMSD graph of MD simulations studies of **AVB4** with MAO-B for 30 ns, and **D**) interactions of **AVB4** with the active site residues of MAO-B during 30 ns MD simulation studies.

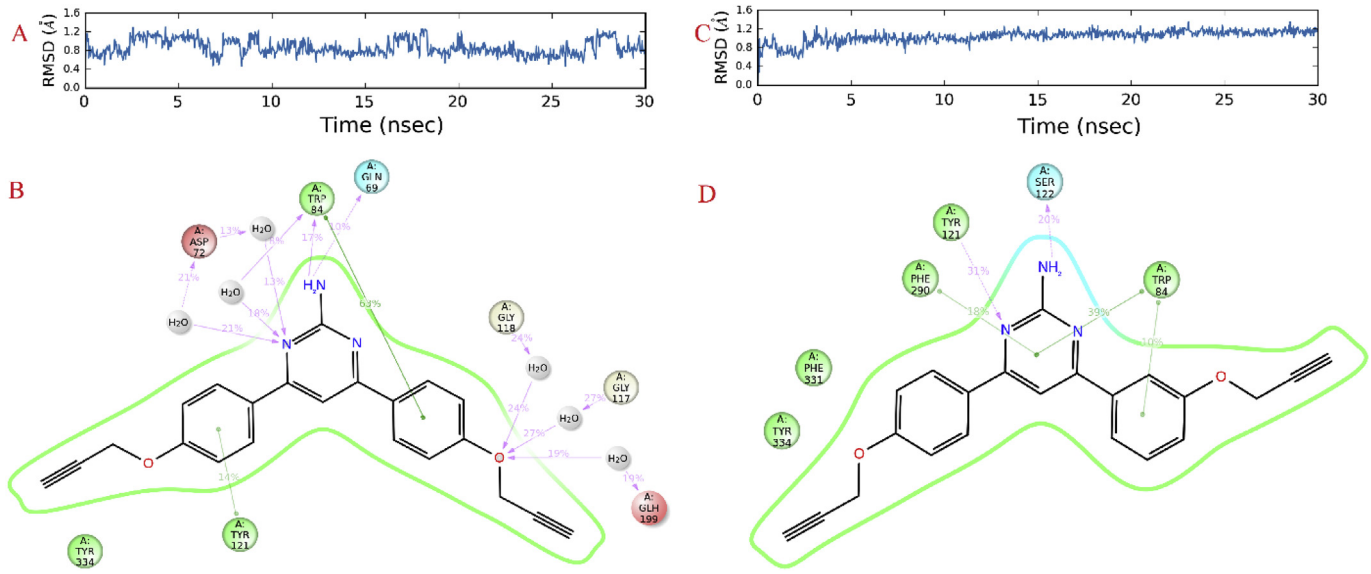

Fig. 10. A) RMSD graph of MD simulations studies of **AVB1** with AChE for 30 ns, **B**) interactions of **AVB1** with the active site residues of AChE during 30 ns MD simulation studies, **C)** RMSD graph of MD simulations studies of **AVB4** with AChE for 30 ns, and **D**) interactions of **AVB4** with the active site residues of AChE during 30 ns MD simulation studies.

Table 2
Physicochemical properties of some of the potent and selective MAO inhibitors.

Compound number	Mol. Wt.	Log P	HB donor	HB acceptor	% human oral absorption	QPlogBB (Optimum range −3.0 to 1.2)	BBB permeability predicted
AVB1	355.39	4.52	3	4	100	−0.934	+ve
AVB4	355.39	4.51	3	4	100	−0.93	+ve

+ ve = blood-brain barrier permeable; - ve = no permeability to the blood-brain barrier.

retained AChE inhibition activity. Replacing NH_2 with phenyl ring in **AVB3** further reduced the MAO-B inhibitory activity by almost 4-folds and AChE inhibition activity by more than 5-folds. Shifting of one of the propargyl group from para (**AVB1**) to meta position (**AVB4**) significantly increased MAO-B inhibitory activity by more than 2-folds and retained AChE inhibition activity. **AVB4** was found to be the most potent MAO-B inhibitor in the series with an IC_{50} value of 1.49 ± 0.09 μM. Replacement of NH_2 group of **AVB4** by CH_3 (**AVB5**) and phenyl (**AVB6**) groups reduced the MAO-B inhibitory activity by more than 5-folds and 12-folds respectively and AChE inhibitory activity was reduced by about 3-folds. Shifting of propargyl group from meta (**AVB4**) to ortho position (**AVB7** to **AVB9**) of the phenyl ring proved detrimental and the MAO-B inhibitory activity was found to be reduced by more than 14-folds. Similarly, reduced MAO-B inhibitory activity was observed when both the phenyl rings were substituted by propargyl groups at the meta positions (**AVB10** and **AVB11**) and at ortho positions (**AVB12** and **AVB13**). Presence of additional substituents at the phenyl ring (**AVB14** to **AVB19**) was also found unfavorable for the MAO-B and AChE inhibitory activities.

3. Conclusion

Multi-targeting agents can be an effective strategy for the treatment of multifactorial diseases like AD. Multi-targeting ligands which can simultaneously target MAO and AChE enzymes are being developed for the treatment of AD. In the current research work, a series of dipropargyl substituted diphenylpyrimidines, have been synthesized and evaluated for MAO and AChE inhibition activities. Most of the compounds were found to be selective inhibitors of MAO-B isoform and potent AChE inhibitors. In the series, **AVB1** and **AVB4** were found to be the most potent inhibitors of AChE and MAO-B with IC_{50} values of 1.35 ± 0.03 μM and 1.49 ± 0.09 μM respectively. In the reversible inhibition studies, the lead compounds were found to be reversible inhibitors of MAO-B and AChE enzymes. In the ROS protection inhibition studies, **AVB1** and **AVB4** displayed weak but interesting activity in SH-SY5Y cells and **AVB1** reduced the ROS levels up to 30% at 5 μM. In the cytotoxicity studies involving SH-SY5Y cells, both **AVB1** and **AVB4** were found to be non-toxic to the tissue cells. In the molecular dynamic simulation studies, the lead compounds were found to be stable in the active site of MAO-B and AChE for the time interval of 30 ns. The results suggested that **AVB1** and **AVB4** are promising dual inhibitors and have the potential to be developed as anti-Alzheimer's drug.

4. Experimental

4.1. Material and methods

All the reagents or chemicals used for the synthesis of intermediates or target compounds were purchased from Avra synthesis, Sigma-Aldrich, Loba-Chemie Pvt. Ltd. and S.D. Fine Chemicals and are used without further purification. Thin layer chromatography was done on glass silica plates with silica gel GF254 as the adsorbent. Ethyl acetate: petroleum ether (1:1, 1:2 and 1:3) mixtures were used as a solvent system for the chromatographic purification of compounds using column chromatography. Mass spectra were recorded on GC-MS (ESI), Central Instruments Laboratory (CIL), Central University of Punjab, Bathinda. The ^{1}H and ^{13}C NMR of the compounds were recorded on JEOL or Bruker Advance II instrument at 400 MHz frequency, in $CDCl_3$ or DMSO and TMS ($\delta = 0$) as an internal standard at IIT Ropar, and GJUS&T, Hisar. The chemical shifts are reported in parts per million (δ) downfield from the signal of tetramethylsilane added to the

deuterated solvent. Melting points were recorded with Stuart SMP30 melting point apparatus and are uncorrected. For MAO inhibition studies and acetylcholinesterase inhibition studies, Amplex® Red MAO kit was purchased from Molecular Probes (Invitrogen), Life technologies, India. Recombinant hMAO-A and hMAO-B enzymes were purchased from Sigma-Aldrich. For absorption studies, UV-VIS spectrophotometer of Shimadzu was used. Fluorescence studies were recorded using Biotek Microplate reader. Molecular modelling studies were carried out using Maestro 11.1 (Schrödinger LLC) and ChemBio Draw Ultra-12 installed on operating system centos 6.5 at HP-2800 workstation with configuration of Intel (R) Xenon (R) X5660 @2.80 GHz, 2.789 GHz (2 processors).

4.2. Chemistry

4.2.1. General procedure for the synthesis of O-propargylated derivatives 3 and 4

To hydroxy substituted acetophenones (0.5g) or benzaldehydes (0.5g), Propargyl bromide (1.2eq) was added in the presence of potassium carbonate as a base (2.4eq.) and acetone (30 ml) as solvent. The reaction mixture was refluxed overnight at 60 °C. Progress of the reaction was monitored via TLC. After completion of the reaction, excess of solvent was evaporated from the mixture using vacuum rotary evaporator, water (10 mL) was added and aqueous phase was extracted with ethyl acetate (10 mL × 3), and washed with brine, dried over anhydrous Na_2SO_4 and the organic solvent was concentrated under vacuum using rotary evaporator to obtain **3** and **4**.

4.2.2. General procedure for the synthesis of 5

To a mixture of **3** (1 eq.) and **4** (1 eq.) in methanol (20 ml), aqueous sodium hydroxide (20%) was added slowly with continuous stirring. The reaction mixture was stirred for 3 h at room temperature. The completion of reaction was monitored via TLC. After completion of reaction, excess of solvent was evaporated from the mixture using rotary evaporator. Chilled water was poured into the reaction mixture and precipitates of **5** were filtered and dried. Further crude product was recrystallized from ethanol or purified using column chromatography as per requirement.

4.2.3. General procedure for the synthesis of AVB1-19

To a mixture of **5** (500 mg), and amidine (1.2 eq.), anhydrous sodium carbonate (2.4 eq.) was added in acetonitrile (10 mL) as solvent. The reaction mixture was refluxed for 24 h at 85 °C. The progress of the reaction was monitored via TLC. After completion of the reaction, excess of solvent was evaporated under vacuum using rotary evaporator, and water (10 mL) was added which was extracted with ethyl acetate (3 × 10 mL), washed with brine, dried over anhydrous Na_2SO_4, and the organic solvent was concentrated under vacuum using rotary evaporator and purified via column chromatography (EtOAc:Pet ether). The final products were characterized by NMR spectroscopy and HRMS.

4,6-bis(4-(prop-2-yn-1-yloxy)phenyl)pyrimidin-2-amine (AVB1): Yield: 55%; yellow solid, mp 139–141 °C; ^{1}H NMR ($CDCl_3$, 400 MHz, δ with TMS = 0): 8.02 (4H, d, J = 8Hz), 7.34 (1H, s), 7.06 (4H, d, J = 8Hz), 5.17 (2H, s), 4.76 (4H, d, J = 4Hz), 2.54 (2H, t, J = 4Hz), ^{13}C NMR ($CDCl_3$, 100 MHz, δ with TMS = 0) δ: 165.40, 163.57, 159.49, 131.16, 128.66, 115.25, 103.02, 76.81, 75.98, 55.92, **HRMS**: for $C_{22}H_{17}N_3O_2$, calculated $[M+H]^+$: 356.1399; observed $[M+H]^+$: 356.1368.

2-methyl-4,6-bis(4-(prop-2-yn-1-yloxy)phenyl)pyrimidine (AVB2): Yield: 60%; blue solid, mp 158–160 °C; ^{1}H NMR ($CDCl_3$, 400 MHz, δ with TMS = 0): 8.10 (4H, d, J = 8Hz), 7.76 (1H, s), 7.10 (4H, d, J = 8Hz), 4.76 (4H, d, J = 4Hz), 2.81 (3H, s), 2.55 (2H, t, J = 4Hz), ^{13}C NMR ($CDCl_3$, 100 MHz, δ with TMS = 0) δ: 168.34, 164.00, 159.59, 130.92, 128.71, 115.21, 108.55, 78.15, 75.90, 55.89, 26.49, **HRMS**: for $C_{23}H_{18}N_2O_2$, calculated $[M+H]^+$: 355.1447; observed $[M+H]^+$: 355.1402.

2-phenyl-4,6-bis(4-(prop-2-yn-1-yloxy)phenyl)pyrimidine (AVB3): Yield: 65%; greenish solid, mp 148–150 °C; ^{1}H NMR ($CDCl_3$, 400 MHz, δ with TMS = 0) 8.73 (2H, d, J = 8Hz), 8.30 (4H, d, J = 8Hz), 7.92 (1H, s), 7.55 (3H, m), 7.18 (4H, d, J = 8Hz), 4.82 (4H, d, J = 4Hz), 2.59 (2H, t, J = 4Hz), ^{13}C NMR ($CDCl_3$, 100 MHz, δ with TMS = 0): 163.90, 159.70, 138.32, 130.98, 130.51, 128.75, 128.40, 115.17, 108.78, 78.17, 75.92, 55.90, **HRMS**: for $C_{28}H_{20}N_2O_2$, calculated $[M+H]^+$: 417.1603; observed $[M+H]^+$: 417.1549.

4-(3-(prop-2-yn-1-yloxy)phenyl)-6-(4-(prop-2-yn-1-yloxy) phenyl)pyrimidin-2-amine (AVB4): Yield: 65%; white solid, mp 139–141 °C; ^{1}H NMR ($CDCl_3$, 400 MHz, δ with TMS = 0): 8.02 (2H, d, J = 8Hz), 7.69-7.63 (2H, m), 7.42 (1H, d, J = 8Hz),7.37 (1H, s), 7.11 - 7.04 (3H, m), 5.25 (2H, s), 4.75 (4H, d, J = 4 Hz), 2.54 (2H, t, J = 4 Hz), ^{13}C NMR ($CDCl_3$, 100 MHz, δ with TMS = 0) δ: 165.66, 163.57, 159.59, 158.02, 139.47, 130.98, 129.90, 128.69, 120.45, 117.15, 115.11, 113.52 103.82, 78.49, 75.81, 56.04, 55.93, **HRMS**: for $C_{22}H_{17}N_3O_2$, calculated $[M+H]^+$: 356.1399; observed $[M+H]^+$: 356.1350.

2-methyl-4-(3-(prop-2-yn-1-yloxy)phenyl)-6-(4-(prop-2-yn-1-yloxy)phenyl)pyrimidine (AVB5): Yield: 63%; white solid, mp 116–118 °C; ^{1}H NMR ($CDCl_3$, 400 MHz, δ with TMS = 0) 8.15 (2H, d, J = 8Hz), 7.83 (1H, s), 7.78 (2H, d, J = 8Hz), 7.47 (1H, t, J = 8Hz), 7.15 (3H, m), 4.83 (4H, d, J = 4Hz), 2.86(3H, s), 2.58 (2H, t, J = 4Hz), ^{13}C NMR (CDCl3, 100 MHz, δ with TMS = 0): 164.27, 158.10, 139.22, 129.98, 128.75, 120.49, 117.14, 115.24, 113.73, 109.44, 78.37, 78.19, 75.92, 75.72, 56.04, 55.88, 26.48, **HRMS**: for $C_{23}H_{18}N_2O_2$, calculated $[M+H]^+$: 355.1447; observed $[M+H]^+$: 355.1390.

2-phenyl-4-(3-(prop-2-yn-1-yloxy)phenyl)-6-(4-(prop-2-yn-1-yloxy)phenyl)pyrimidine (AVB6): Yield: 60%; white solid, mp 147–148 °C; ^{1}H NMR ($CDCl_3$, 400 MHz, δ with TMS = 0): 8.72-8.70 (2H, m), 8.2 (2H, d, J = 8 Hz), 7.97-7.85 (3H, m), 7.54-7.48 (4H, m), 7.15 (3H, d, J = 8Hz), 4.83 (4H, d, J = 2.4 Hz), 2.59 (2H, m); ^{13}C NMR ($CDCl_3$, 100 MHz, δ with TMS = 0) δ: 164.38, 164.18, 164.11, 159.84, 158.18, 139.28, 138.20, 130.82, 130.72, 130.02, 128.87, 128.52, 120.50, 117.18, 115.24, 113.96, 109.70, 78.50, 76.06, 56.13, 55.95, **HRMS**: for $C_{28}H_{20}N_2O_2$, calculated $[M+H]^+$: 417.1603; observed $[M+H]^+$: 417.1553.

4-(2-(prop-2-yn-1-yloxy)phenyl)-6-(4-(prop-2-yn-1-yloxy) phenyl)pyrimidin-2-amine (AVB7): Yield: 64%; green solid, mp 134–136 °C; ^{1}H NMR ($CDCl_3$, 400 MHz, δ with TMS = 0) 8.07 (2H, d, J = 8Hz), 7.90 (1H, d, J = 8Hz), 7.66 (1H, s), 7.45 (1H, t, J = 8Hz), 7.18 (2H, d, J = 8Hz), 7.09 (2H, d, J = 8Hz), 5.15 (2H, bs), 4.79 (4H, t, J = 4Hz), 2.57 (2H, t, J = 4Hz), ^{13}C NMR ($CDCl_3$, 100 MHz, δ with TMS = 0): 164.54, 164.29, 163.34, 159.39, 155.67, 131.21, 130.87, 128.72, 128.21, 122.15, 114.95, 113.54, 108.57, 78.46, 78.23, 76.70, 75.83, 56.66, 55.85, 29.70, **HRMS**: for $C_{22}H_{17}N_3O_2$, calculated $[M+H]^+$: 356.1399; observed $[M+H]^+$: 356.1372.

2-methyl-4-(2-(prop-2-yn-1-yloxy)phenyl)-6-(4-(prop-2-yn-1-yloxy)phenyl)pyrimidine (AVB8): Yield: 58%; green solid, mp 132–134 °C; ^{1}H NMR ($CDCl_3$, 400 MHz, δ with TMS = 0) 8.13 (3H, t, J = 8Hz), 7.99 (1H, d, J = 8Hz), 7.47 (1H, t, J = 8Hz),7.17 (4H, m), 4.80 (4H, d, J = 4Hz), 2.86 (3H, s), 2.58 (2H, t, J = 4Hz), ^{13}C NMR (CDCl3, 100 MHz, δ with TMS = 0): 168.04, 163.14, 162.88, 159.49, 155.73, 131.22, 131.12, 131.08, 130.77, 128.85, 127.88, 122.30, 115.12, 114.64, 114.25, 113.34, 78.37, 78.19, 75.91, 75.86, 56.62, 55.86, 26.53, **HRMS**: for $C_{23}H_{18}N_2O_2$, calculated $[M+H]^+$: 355.1447; observed $[M+H]^+$: 355.1405.

2-phenyl-4-(2-(prop-2-yn-1-yloxy)phenyl)-6-(4-(prop-2-yn-1-yloxy)phenyl)pyrimidine (AVB9): Yield: 65%; cream solid, mp 89–91 °C; ^{1}H NMR ($CDCl_3$, 400 MHz, δ with TMS = 0): 8.67 (2H, dd, J_{13} = 8 Hz; J_{12} = 4 Hz), 8.29-8.25 (4H, m), 7.52 - 7.46 (4H, m), 7.24 - 7.19 (1H, m), 7.15-7.11 (3H, m); 4.77 (4H, d, J = 4 Hz), 2.54 (2H, t, J = 4Hz), ^{13}C NMR ($CDCl_3$, 100 MHz, δ with TMS = 0) δ: 164.18,

163.16, 162.83, 159.66, 156.18, 138.51, 131.61, 131.22, 130.47, 128.98, 128.48, 127.86 122.34, 115.14, 114.86, 113.49, 78.48, 76.82, 56.73, 55.94, **HRMS**: for $C_{28}H_{20}N_2O_2$, calculated $[M+H]^+$: 417.1603; observed $[M+H]^+$: 417.1555.

4,6-bis(3-(prop-2-yn-1-yloxy)phenyl)pyrimidin-2-amine (AVB10): Yield: 57%; yellowish brown, mp 146–148 °C; ^{1}H NMR ($CDCl_3$, 400 MHz, δ with TMS = 0): 7.72 (2H, s), 7.69 (2H, d, J = 8Hz), 7.45 (3H, t, J = 8Hz), 7.14 (2H, d, J = 8Hz), 5.21 (2H, bs), 4.81 (4H, d, J = 4 Hz), 2.58 (2H, bs), ^{13}C NMR ($CDCl_3$, 100 MHz, δ with TMS = 0) δ: 165.84, 163.50, 157.98, 139.23, 129.86, 120.39, 117.22, 113.46, 104.53, 78.40, 75.74, 55.99, 29.86, **HRMS**: for $C_{22}H_{17}N_3O_2$, calculated $[M+H]^+$: 356.1399; observed $[M+H]^+$: 356.1358.

2-phenyl-4,6-bis(3-(prop-2-yn-1-yloxy)phenyl)pyrimidine (AVB11): Yield: 59%; greenish yellow solid, mp 118–120 °C; ^{1}H NMR ($CDCl_3$, 400 MHz, δ with TMS = 0) 8.75 (2H, d, J = 8Hz), 8.45 (1H, s) 8.01 (2H, d, J = 8Hz), 7.59 (1H, s), 7.57 (2H, d, J = 8Hz), 7.50–7.59 (4H, m), 7.20 (2H, d, J = 8Hz), 4.86 (4H, d, J = 4Hz), 2.62 (2H, t, J = 4Hz), ^{13}C NMR (CDCl3, 100 MHz, δ with TMS = 0): 164.43, 164.35, 158.15, 139.05, 137.98, 130.74, 129.98, 128.48, 120.48, 117.28, 113.94, 110.51, 78.40, 75.86, 56.08, 29.71, **HRMS**: for $C_{28}H_{20}N_2O_2$, calculated $[M+H]^+$: 417.1603; observed $[M+H]^+$: 417.1602.

4,6-bis(2-(prop-2-yn-1-yloxy)phenyl)pyrimidin-2-amine (AVB12): Yield: 64%; semi-solid; ^{1}H NMR ($CDCl_3$, 400 MHz, δ with TMS = 0) 7.83 (2H, d, J = 8Hz), 7.68 (1H, s), 7.44 (2H, t, J = 8Hz), 7.13–7.19 (4H, m), 5.47 (2H, bs), 4.80 (4H, d, J = 4Hz), 2.53 (2H, bs), ^{13}C NMR (CDCl3, 100 MHz, δ with TMS = 0): 163.79, 163.19, 155.55, 131.04, 130.80, 128.25, 122.00, 113.73, 113.56, 78.58, 75.86, 56.47, 29.72, **HRMS**: for $C_{22}H_{17}N_3O_2$, calculated $[M+H]^+$: 356.1399; observed $[M+H]^+$: 356.1368.

2-phenyl-4,6-bis(2-(prop-2-yn-1-yloxy)phenyl)pyrimidine (AVB13): Yield: 68%; semi-solid; ^{1}H NMR ($CDCl_3$, 400 MHz, δ with TMS = 0) 8.69 (2H, d, J = 8Hz), 8.49 (1H, s), 8.24 (2H, d, J = 8Hz), 7.49–7.54 (5H, m), 7.22–7.27 (4H, m), 4.87 (4H, d, J = 4Hz), 2.55 (2H, bs), ^{13}C NMR (CDCl3, 100 MHz, δ with TMS = 0): 164.08, 162.32, 156.01, 138.53, 131.70, 131.10, 130.27, 128.38, 128.29, 128.22, 122.15, 120.46, 113.56, 78.57, 75.95, 56.48, 29.74, **HRMS**: for $C_{28}H_{20}N_2O_2$, calculated $[M+H]^+$: 417.1603; observed $[M+H]^+$: 417.1552.

4-(3-methoxy-4-(prop-2-yn-1-yloxy)phenyl)-6-(4-(prop-2-yn-1-yloxy)phenyl)pyrimidin-2-amine (AVB14): Yield: 60%; light brown solid, mp 118–120 °C; ^{1}H NMR ($CDCl_3$, 400 MHz, δ with TMS = 0): 8.04 (2H, d, J = 8Hz), 7.69 (1H, d, J = 8Hz), 7.60-7.58 (1H, m), 7.35 (1H, s), 7.12-7.06 (3H, m), 5.29 (2H, S), 4.83 (2H, d, J = 4Hz), 4.76 (2H, d, J = 4Hz), 3.99 (3H, s), 2.55 (2H, t, J = 4Hz), ^{13}C NMR ($CDCl_3$, 100 MHz, δ with TMS = 0) δ: 165.41, 163.47, 159.49, 149.78, 148.82, 131.73, 131.01, 128.63, 119.84, 115.04, 113.65, 110.48, 103.17, 78.19, 76.73, 75.09, 56.68, 56.06, 55.87, **HRMS**: for $C_{23}H_{19}N_3O_3$, calculated $[M+H]^+$: 386.1505; observed $[M+H]^+$: 386.1508.

4-(3-methoxy-4-(prop-2-yn-1-yloxy)phenyl)-2-methyl-6-(4-(prop-2-yn-1-yloxy)phenyl)pyrimidine (AVB15): Yield: 60%; white solid, mp 132–134 °C; ^{1}H NMR ($CDCl_3$, 400 MHz, δ with TMS = 0): 8.10 (2H, d, J = 8H), 7.77 (2H, s), 7.66 (1H, dd, J_{13} = 8Hz, J_{12} = 4Hz), 7.15–7.09 (3H, m), 4.84 (2H, d, J = 4Hz), 4.77 (2H, d, J = 4Hz), 4.01 (3H, s), 2.82 (3H, s), 2.56-2.53 (2H, t, J = 4Hz), ^{13}C NMR ($CDCl_3$, 100 MHz, δ with TMS = 0) δ: 168.34, 164.05, 164.03, 157.60, 149.97, 148.97, 131.62, 130.88, 128.72, 119.93, 115.22, 113.83, 110.56, 108.74, 78.16 78.14, 76.18, 75.92, 56.71, 56.12, 55.80, 26.50, **HRMS**: for $C_{24}H_{20}N_2O_3$, calculated $[M+H]^+$: 385.1552; observed $[M+H]^+$: 386.1555.

4-(3-methoxy-4-(prop-2-yn-1-yloxy)phenyl)-2-phenyl-6-(4-(prop-2-yn-1-yloxy)phenyl)pyrimidine (AVB16): Yield: 70%; greenish white solid, mp 160–162 °C; ^{1}H NMR ($CDCl_3$ and DMSO, 400 MHz, δ with TMS = 0): 8.64 (2H, d, J = 8Hz), 8.45 (2H, d, J = 8 Hz), 8.29 (1H, s), 8.05 - 8.01 (2H, m), 7.58 - 7.52 (3H, m), 7.18 (3H, m), 4.88 (4H, d, J = 4 Hz), 4.00 (3H, s), 3.36 (2H, t, J = 4Hz), ^{13}C NMR ($CDCl_3$ and DMSO, 100 MHz, δ with TMS = 0) δ: 163.39, 163.31, 163.03, 159.47, 149.32, 148.96, 137.74, 130.39, 130.37, 129.81, 128.76, 128.36, 127.86, 120.19, 114.85, 113.59, 110.62, 108.89, 79.88, 78.67, 78.58, 77.84, 56.11, 55.72, 55.55, **HRMS**: for $C_{29}H_{22}N_2O_3$, calculated $[M+H]^+$: 447.1709; observed $[M+H]^+$: 447.1709.

4-(3-ethoxy-4-(prop-2-yn-1-yloxy)phenyl)-6-(4-(prop-2-yn-1-yloxy)phenyl)pyrimidin-2-amine (AVB17): Yield: 65%; pale yellow solid, mp 162–164 °C; ^{1}H NMR ($CDCl_3$, 400 MHz, δ with TMS = 0) 8.05 (2H, d, J = 8Hz), 7.71 (1H, s), 7.62 (1H, d, J = 8Hz), 7.38 (1H, s), 7.16 (1H, d, J = 8Hz), 7.13 (2H, d, J = 8Hz), 5.21 (2H, bs), 4.87 (2H, d, J = 4Hz), 4.80 (2H, d, J = 4Hz), 4.26 (2H, q, J = 8Hz), 2.57 (2H, m), 1.53 (3H, t, J = 4Hz), ^{13}C NMR (CDCl3, 100 MHz, δ with TMS = 0): 165.51, 165.36, 163.42, 159.47, 149.27, 149.12, 131.83, 131.05, 128.60, 119.83, 115.03, 114.42, 112.00, 103.20, 78.43, 78.17, 75.99, 75.66, 64.64, 56.85, 55.87, 30.27, 29.67, 14.86, **HRMS**: for $C_{24}H_{21}N_3O_3$, calculatSed $[M+H]^+$: 400.1661; observed $[M+H]^+$: 400.1665.

4-(3-ethoxy-4-(prop-2-yn-1-yloxy)phenyl)-2-methyl-6-(4-(prop-2-yn-1-yloxy)phenyl)pyrimidine (AVB18): Yield: 60%; greenish yellow solid, mp 108–110 °C; ^{1}H NMR ($CDCl_3$, 400 MHz, δ with TMS = 0) 8.13 (2H, d, J = 8Hz), 7.79 (2H, s), 7.67 (1H, d, J = 4Hz), 7.17 (1H, d, J = 4Hz), 7.13 (2H, d, J = 8Hz), 4.87 (2H, d, J = 4Hz), 4.80 (2H, d, J = 4Hz), 4.28 (2H, q, J = 4Hz), 2.85 (3H, s), 2.57 (2H, m), 1.56 (3H, t, J = 4Hz), ^{13}C NMR (CDCl3, 100 MHz, δ with TMS = 0): 168.33, 164.13, 164.01, 159.59, 149.45, 149.27, 131.68, 130.91, 128.72, 119.94, 115.22, 114.56, 112.09, 108.78, 78.39, 78.14, 76.05, 75.91, 64.71, 56.85, 55.89, 26.50, 14.86, **HRMS**: for $C_{25}H_{22}N_2O_3$, calculated $[M+H]^+$: 399.1709; observed $[M+H]^+$: 399.1709.

4-(3-ethoxy-4-(prop-2-yn-1-yloxy)phenyl)-2-phenyl-6-(4-(prop-2-yn-1-yloxy)phenyl)pyrimidine (AVB19): Yield: 67%; greenish yellow solid, mp 138–140 °C; ^{1}H NMR ($CDCl_3$, 400 MHz, δ with TMS = 0) 8.72 (2H, d, J = 8Hz), 8.30 (2H, d, J = 8Hz), 7.97 (1H, d, J = 4Hz), 7.91 (1H, s), 7.82 (1H, d, J = 8Hz), 7.57 (3H, m), 7.21 (1H, d, J = 8Hz), 7.19 (2H, d, J = 8Hz), 4.90 (2H, d, J = 4Hz), 4.83 (2H, d, J = 4Hz), 4.32 (2H, q, J = 12Hz), 2.65 (2H, dd, J = 4Hz), 1.65 (3H, m) ^{13}C NMR (CDCl3, 100 MHz, δ with TMS = 0): 164.06, 159.72, 149.44, 149.41, 138.29, 131.75, 130.94, 130.54, 128.76, 128.42, 128.39, 120.03, 115.18, 114.52, 112.27, 109.02, 78.40, 78.16, 76.07, 75.93, 64.79, 56.86, 55.90, 14.88, **HRMS**: for $C_{30}H_{24}N_2O_3$, calculated $[M+H]^+$: 461.1865; observed $[M+H]^+$: 461.1866.

4.3. Biological studies

4.3.1. Determination of hMAO inhibition activity

The effects of the test compounds on hMAO-A and hMAO-B enzymes were evaluated by using Amplex® Red assay kit based on detection of fluorescence [32,33].

Briefly, 100 μL of sodium phosphate buffer (0.05 M, pH 7.4) containing the test drugs or reference inhibitors, in various concentrations along with adequate amounts of recombinant hMAO (hMAO-A: 1.1 μg protein; specific activity: 150 nmol of p-tyramine oxidized to p-hydroxyphenylacetaldehyde/min/mg protein; hMAO-B: 7.5 μg protein; specific activity: 22 nmol of p-tyramine transformed/min/mg protein) enzyme, were incubated for 30 min at 37 °C in a flat-black-bottom 96-well plate (Tarsons) in incubator. After this incubation period, the reaction was started by adding (final concentrations) 200 μM Amplex® Red reagent, 1 U/mL horseradish peroxidase and 1 mM p-tyramine. After 30 min incubation in the dark, the production of H_2O_2 was quantified at 37 °C in a multi-detection microplate fluorescence reader (Synergy^{HI}, Bio-Tek® Instruments) based on the fluorescence generated at the excitation wavelength of 545 nm, and emission wavelength of 590 nm. Control experiments were carried out simultaneously by replacing the test drugs with the vehicle. To minimize the possibility of any interference of test drugs to the non-enzymatic fluorescence generated through drug and Amplex® Red reagent

interactions blank reading was taken with drug and Amplex® Red reagent without adding MAO enzyme in a sodium phosphate buffer. No fluorescence could be observed in the absence of MAO enzyme thus eliminating the possibility of any false reading. The specific final fluorescence emission was calculated after subtraction of the background activity, determined from vials containing all components except the hMAO enzyme replaced by a sodium phosphate buffer solution.

4.3.2. Acetylcholinesterase inhibition assay

Acetylcholinesterase inhibition activity was determined using Amplex Red Acetylcholine/Acetylcholinesterase assay kit (A12217) purchased from the Molecular Probes Inc. Invitrogen [15,34]. Briefly, 100 μl of Tris-HCl buffer (0.05 M, pH 8.0) containing the synthesized test drugs and reference inhibitors, in various concentrations along with adequate amounts of recombinant AChE (0.2U/mL) enzyme, were incubated for 15 min at 37 °C in a flat bottom 96-well plates (Tarsons). Reaction was started by adding 100 μl of working solution of 400 μM Amplex Red reagent containing 2 U/mL horseradish peroxidase, 0.2 U/mL choline oxidase and 100 μM acetylcholine. After 30 min incubation in dark, the production of H_2O_2 and subsequent formation of resorufin from Amplex red dye was quantified at 37 °C in a multi-detection microplate fluorescence reader (Synergy^{HI}, Bio-Tek® Instruments) based on the fluorescence generated at excitation wavelength of 545 nm, and emission wavelength of 590 nm. Positive control experiment was carried out simultaneously by replacing the test drugs with the vehicle. Second positive control was carried out by using 20 mM H_2O_2. 1X reaction buffer without acetylcholinesterase was used as negative control. The specific final fluorescence emission was calculated after subtraction of the background activity, determined from wells containing all components except the AChE replaced by a 1X buffer solution. Each experiment was performed in triplicate (n = 3).

4.3.3. Reversibility studies

For reversibility studies, dilution protocol was adopted as reported in the literature [35,36]. Briefly, the test inhibitors were incubated with the MAO enzyme at concentrations of 10 × IC_{50} and 100 × IC_{50} at 37 °C for of 30 min (negative control performed in the absence of inhibitor), and 4% DMSO was added as co-solvent to all incubations. After 30 min incubation period, the samples were subsequently diluted to 100−fold with the addition of tyramine substrate to achieve final inhibitor concentrations of 0.1 × IC_{50} and 1 x IC_{50} value, respectively. As positive control MAO-B was incubated with the irreversible inhibitor pargyline at 10 × IC_{50} concentrations and then diluted 100-fold to achieve final inhibitor concentrations of 0.1 × IC_{50}. The residual MAO-B activity was measured (n = 3) after dilutions and enzyme activities were expressed as mean ± SD.

4.3.4. Kinetic studies

To determine the mechanism of action of the most potent inhibitor of AChE i.e. **AVB4,** kinetic study was performed using *ee*AChE with the help of earlier reported protocols [18,37]. Lineweaver-Burk double reciprocal graph was plotted at different concentrations of substrate ACh (0.1 mM- 1 mM) by using same methodology reported for the *in vitro* inhibition study of AChE. Progress curves were analyzed by steady-state turnover of substrate and values of linear regression were fitted according to Lineweaver-Burk replots using excel software (2016). Three concentrations of **AVB4** (1 μM, 2 μM and 5 μM) were used for the kinetic study. The plots were assessed by weighted least-square analysis that assumed the variance of ν to be constant for whole data set. Slopes of the reciprocal of ν were then plotted against the reciprocal of the substrate concentration.

4.3.5. Cell culture and treatment

The human neuroblastoma (SH-SY5Y) cells were obtained from National Centre for Cell Science (Pune, India). The cells were routinely grown in DMEM supplemented with 10% FBS (Biological Industries) and 1XxPSN mix (Invitrogen) at 37 °C in a humidified atmosphere containing 5% CO_2. Cells were subcultured by trypsinization and seeded in 96 and 24 well plates according to the requirement of the experiments.

4.3.6. ROS inhibition studies

Intracellular levels of ROS were determined by using the protocol described elsewhere [15], using non-fluorescent compound 2,7-dichlorofluorescein diacetate (DCF-DA) that is permeable to the cell membrane where it is hydrolyzed by intracellular esterases and oxidized by ROS to a fluorescent compound 2,7-DCF. The human neuroblastoma (SH-SY5Y) cells (approximately 10,000 cells/well) were seeded of 96 well plate in DMEM/F-12 media containing 10% FBS and horse serum supplemented 1% penicillin antibiotic solution for 24h in a humidified atmosphere containing 5% CO_2. The media was removed, washed with PBS and cells were treated with test compounds (without FBS) for 24 h at different concentrations (1 μM, 5 μM and 25 μM). Thereafter, cells were rinsed with PBS three times and treated with H_2DCF-DA (50 μM) and incubated for 30 min at 37 °C. Following incubation, cells were rinsed with PBS and fluorescence was detected at a wavelength of 478 nm excitation and 518 nm emission.

4.3.7. Neuroprotective studies

The neuroprotective potential of compounds was determined against 6-OHDA neurotoxin using MTT assay [38]. For this SH-SY5Y cells were plated in 96 wells, at 10^4 cells/well density. The cells were cultured for 24h in DMEM/F-12 media containing 10% FBS and horse serum supplemented 1% penicillin antibiotic solution. Then cells were treated with the target compounds (at concentrations of 1−25 μM), 4h before 6-OHDA (10 μM). After 24 h incubation in the oven, at 37 °C and a 5% CO_2, 95% O_2 atmosphere, the tested compounds were replaced with 100 μL of MTT in media (5 mg/mL, final concentration). The cells were incubated for another 3h. After the removal of MTT, the formazan crystals were dissolved in DMSO. The amount of formazan was measured using a microculture plate reader with a test wavelength of 594 nm. Results were expressed as the mean ± SD of three independent experiments.

4.3.8. Cytotoxicity studies

With an aim to test the cytotoxicity of the synthesized compounds, studies were carried out with human neuroblastoma SH-SY5Y cells, using the 3-(4, 5-dimethylthiazol-2-yl)-2, 5-diphenyltetrazolium bromide (MTT) test [38]. This method is based on the formation of blue formazan product by the cellular oxidoreductase. The amount of formazan produced is considered as a reliable representation of viable cell number. Approximately 10,000 cells were seeded per well of 96 well plate in DMEM/F-12 media containing 10% FBS and horse serum supplemented 1% penicillin antibiotic solution for 24h and treated as indicated in the experimental design. Cells were treated with synthesized compounds at concentration of 1 μM, 5 μM and 25 μM for 24h in humidified CO_2 incubator, maintained at 37 °C with 5% CO_2 and 95% humidity under serum-free conditions. After 4 h incubation at 37 °C, this solution was removed, and the resulting blue formazan was solubilized in 100 ml of DMSO and the optical density was recorded at 595 nm using microplate reader.

4.4. Computational studies

4.4.1. Molecular docking studies

To determine the mode of interaction between synthesized ligands and the active site of hMAO-A and hMAO-B enzymes, molecular docking studies were performed using Glide [39] module of Maestro 11.1 (Schrödinger LLC). X-ray crystal structures of hMAO-B (PDB ID- 2BYB) [30] and AChE (PDB ID- 1EVE) [31] enzymes were imported from the protein data bank (www.rscb.org). Protein was prepared using "protein preparation wizard" application of Schrödinger suite 2017. The energy was minimized using an OPLS2005 force field. The grid was generated (20 Å) around the co-crystallized ligand using receptor grid generation module of Maestro 11.1. Ligands were drawn in ChemBio Draw Ultra-12 (2D SDF) and prepared (3D Maestro input files) using ligand preparation application in Schrödinger suite 2017. In this module, hydrogens were attached, possible ionization states were generated at pH 7.4, possible tautomer for each structure were generated and lowest energy conformation for each possible structural conformation was generated using OPLS2005 force field. For each compound, the top-score docking poses were chosen for final ligand-target interaction analysis employing XP interaction visualizer of Maestro 11.1 software. Validation of docking procedure was first evaluated by re-docking of the co-crystalized ligand into the active site of MAO enzyme. Qikprop [40] application of Schrodinger suit was used to determine the drug like and ADME properties of the compounds.

4.4.2. Molecular dynamics simulation studies

In order to investigate the behavior and stability of the potent inhibitors into the active site of the MAO and AChE, molecular dynamic (MD) simulation was utilized. For this docking complexes of **AVB1** and **AVB4** with MAO-B and AChE were used. MD simulations were performed using Desmond standard protocol [41]. Complex was solvated by TIP3P water model and then naturalized by adding 0.15M Na^+ and Cl^- ions. The thickness of water layer was set to 10 Å. Before the MD simulations the systems were minimized with a maximum iteration of 2000 steps. Then, the systems were submitted to 30 ns MD simulation for equilibration and production MD run. Temperature and pressure were assigned on 300 K and 1.01325 bar, respectively using Isothermal–isobaric (NPT) ensemble. Cut-off radios of 9 Å was used for Coulomb interactions.

Acknowledgement

V.K. is thankful to the DST-SERB (EMR/2015/002339) and Central University of Punjab, Bathinda, (RSM GP25) for providing the financial assistance. B.K. is thankful to CUP, Bathinda and CSIR for the Senior Research Fellowship. Vijay Kumar is thankful to UGC for NET-JRF. J.P. is thankful to DST-SERB for the Research Grant (ECR/2015/000240).

Appendix A. Supplementary data

Supplementary data to this article can be found online at https://doi.org/10.1016/j.ejmech.2019.05.039.

Conflicts of interest

A provisional patent application has been filed containing these compounds (Indian patent application number 201811008301).

References

[1] M. Goedert, M.G. Spillantini, A century of Alzheimer's disease, Science 314 (2006) 777–781.
[2] J.T. Coyle, P. Puttfarcken, Oxidative stress, glutamate, and neurodegenerative disorders, Science 262 (1993) 689–695.
[3] J. Rodda, J. Carter, Cholinesterase inhibitors and memantine for symptomatic treatment of dementia, BMJ 344 (2012), e2986.
[4] G. Reid, N. Chilukuri, S. Darvesh, Butyrylcholinesterase and the cholinergic system, Neuroscience 234 (2013) 53–68.
[5] A.V. Terry Jr., J.J. Buccafusco, C. Wilson, Cognitive dysfunction in neuropsychiatric disorders: selected serotonin receptor subtypes as therapeutic targets, Behav. Brain Res. 195 (2008) 30–38.
[6] Z. Cai, Monoamine oxidase inhibitors: promising therapeutic agents for Alzheimer's disease, Mol. Med. Rep. 9 (2014) 1533–1541.
[7] M. Bortolato, K. Chen, J.C. Shih, Monoamine oxidase inactivation: from pathophysiology to therapeutics, Adv. Drug Deliv. Rev. 60 (2008) 1527–1533.
[8] R.W. Fuller, Selectivity among monoamine oxidase inhibitors and its possible importance for development of antidepressant drugs, Prog. Neuro Psychopharmacol. 2 (1978) 303–311.
[9] P. Riederer, M.B. Youdim, Monoamine oxidase activity and monoamine metabolism in brains of parkinsonian patients treated with l-deprenyl, J. Neurochem. 46 (1986) 1359–1365.
[10] B. Kumar, A.K. Mantha, V. Kumar, Recent developments on the structure–activity relationship studies of MAO inhibitors and their role in different neurological disorders, RSC Adv. 6 (2016) 42660–42683.
[11] M. Naoi, W. Maruyama, Functional mechanism of neuroprotection by inhibitors of type B monoamine oxidase in Parkinson's disease, Expert Rev. Neurother. 9 (2009) 1233–1250.
[12] O. Bar-Am, T. Amit, M.B. Youdim, Aminoindan and hydroxyaminoindan, metabolites of rasagiline and ladostigil, respectively, exert neuroprotective properties in vitro, J. Neurochem. 103 (2007) 500–508.
[13] D.J. Selkoe, Alzheimer's disease: genes, proteins, and therapy, Physiol. Rev. 81 (2001) 741–766.
[14] J. Hardy, D.J. Selkoe, The amyloid hypothesis of Alzheimer's disease: progress and problems on the road to therapeutics, Science 297 (2002) 353–356.
[15] B. Kumar, A.R. Dwivedi, B. Sarkar, S.K. Gupta, S. Krishnamurthy, A.K. Mantha, J. Parkash, V. Kumar, 4, 6-diphenylpyrimidine derivatives as dual inhibitors of monoamine oxidase and acetylcholinesterase for the treatment of Alzheimer's disease, ACS Chem. Neurosci. 10 (2019) 252–265.
[16] B. Kumar, V. Prakash Gupta, V. Kumar, A perspective on monoamine oxidase enzyme as drug target: challenges and opportunities, Curr. Drug Targets 18 (2017) 87–97.
[17] A. Samadi, M. Chioua, I. Bolea, C. de los Ríos, I. Iriepa, I. Moraleda, A. Bastida, G. Esteban, M. Unzeta, E. Gálvez, Synthesis, biological assessment and molecular modeling of new multipotent MAO and cholinesterase inhibitors as potential drugs for the treatment of Alzheimer's disease, Eur. J. Med. Chem. 46 (2011) 4665–4668.
[18] I. Bolea, J. Juarez-Jiménez, C.b. de los Rıos, M. Chioua, R.n. Pouplana, F.J. Luque, M. Unzeta, J. Marco-Contelles, A. Samadi, Synthesis, biological evaluation, and molecular modeling of donepezil and N-[(5-(benzyloxy)-1-methyl-1 H-indol-2-yl) methyl]-N-methylprop-2-yn-1-amine hybrids as new multipotent cholinesterase/monoamine oxidase inhibitors for the treatment of Alzheimer's disease, J. Med. Chem. 54 (2011) 8251–8270.
[19] A. Samadi, C. de los Ríos, I. Bolea, M. Chioua, I. Iriepa, I. Moraleda, M. Bartolini, V. Andrisano, E. Gálvez, C. Valderas, Multipotent MAO and cholinesterase inhibitors for the treatment of Alzheimer's disease: synthesis, pharmacological analysis and molecular modeling of heterocyclic substituted alkyl and cycloalkyl propargyl amine, Eur. J. Med. Chem. 52 (2012) 251–262.
[20] O.M. Bautista-Aguilera, G. Esteban, I. Bolea, K. Nikolic, D. Agbaba, I. Moraleda, I. Iriepa, A. Samadi, E. Soriano, M. Unzeta, Design, synthesis, pharmacological evaluation, QSAR analysis, molecular modeling and ADMET of novel donepezil–indolyl hybrids as multipotent cholinesterase/monoamine oxidase inhibitors for the potential treatment of Alzheimer's disease, Eur. J. Med. Chem. 75 (2014) 82–95.
[21] O.M. Bautista-Aguilera, A. Samadi, M. Chioua, K. Nikolic, S. Filipic, D. Agbaba, E. Soriano, L. de Andres, M.I. Rodríguez-Franco, S. Alcaro, N-Methyl-N-((1-methyl-5-(3-(1-(2-methylbenzyl) piperidin-4-yl) propoxy)-1 H-indol-2-yl) methyl) prop-2-yn-1-amine, a new cholinesterase and monoamine oxidase dual inhibitor, J. Med. Chem. 57 (2014) 10455–10463.
[22] H. Zheng, M.B. Youdim, M. Fridkin, Site-activated chelators targeting acetylcholinesterase and monoamine oxidase for Alzheimer's therapy, ACS Chem. Biol. 5 (2010) 603–610.
[23] M.-Y. Wu, G. Esteban, S. Brogi, M. Shionoya, L. Wang, G. Campiani, M. Unzeta, T. Inokuchi, S. Butini, J. Marco-Contelles, Donepezil-like multifunctional agents: design, synthesis, molecular modeling and biological evaluation, Eur. J. Med. Chem. 121 (2016) 864–879.
[24] L. Wang, G. Esteban, M. Ojima, O.M. Bautista-Aguilera, T. Inokuchi, I. Moraleda, I. Iriepa, A. Samadi, M.B. Youdim, A. Romero, Donepezil+ propargylamine+ 8-hydroxyquinoline hybrids as new multifunctional metal-chelators, ChE and MAO inhibitors for the potential treatment of Alzheimer's disease, Eur. J. Med. Chem. 80 (2014) 543–561.
[25] F.T. Zindo, J. Joubert, S.F. Malan, Propargylamine as functional moiety in the design of multifunctional drugs for neurodegenerative disorders: MAO inhibition and beyond, Future Med. Chem. 7 (2015) 609–629.
[26] I. Bolea, A. Gella, M. Unzeta, Propargylamine-derived multitarget-directed ligands: fighting Alzheimer's disease with monoamine oxidase inhibitors, J. Neural Transm. 120 (2013) 893–902.

[27] O. Weinreb, T. Amit, O. Bar-Am, M.B. Youdim, Rasagiline: a novel anti-Parkinsonian monoamine oxidase-B inhibitor with neuroprotective activity, Prog. Neurobiol. 92 (2010) 330–344.
[28] M.B. Youdim, O. Bar Am, M. Yogev-Falach, O. Weinreb, W. Maruyama, M. Naoi, T. Amit, Rasagiline: neurodegeneration, neuroprotection, and mitochondrial permeability transition, J. Neurosci. Res. 79 (2005) 172–179.
[29] W. Maruyama, Y. Akao, M.C. Carrillo, K.-i. Kitani, M.B. Youdium, M. Naoi, Neuroprotection by propargylamines in Parkinson's disease: suppression of apoptosis and induction of prosurvival genes, Neurotoxicol. Teratol. 24 (2002) 675–682.
[30] L. De Colibus, M. Li, C. Binda, A. Lustig, D.E. Edmondson, A. Mattevi, Three-dimensional structure of human monoamine oxidase A (MAO A): relation to the structures of rat MAO A and human MAO B, Proc. Natl. Acad. Sci. U.S.A. 102 (2005) 12684–12689.
[31] J. Cheung, M.J. Rudolph, F. Burshteyn, M.S. Cassidy, E.N. Gary, J. Love, M.C. Franklin, J.J. Height, Structures of human acetylcholinesterase in complex with pharmacologically important ligands, J. Med. Chem. 55 (2012) 10282–10286.
[32] F. Chimenti, S. Carradori, D. Secci, A. Bolasco, B. Bizzarri, P. Chimenti, A. Granese, M. Yanez, F. Orallo, Synthesis and inhibitory activity against human monoamine oxidase of N1-thiocarbamoyl-3, 5-di (hetero) aryl-4, 5-dihydro-(1H)-pyrazole derivatives, Eur. J. Med. Chem. 45 (2010) 800–804.
[33] B. Kumar, Sheetal, A.K. Mantha, V. Kumar, Synthesis, biological evaluation and molecular modeling studies of phenyl-/benzhydrylpiperazine derivatives as potential MAO inhibitors, Bioorg. Chem. 77 (2018) 252–262.
[34] A. Kalb, C. von Haefen, M. Sifringer, A. Tegethoff, N. Paeschke, M. Kostova, A. Feldheiser, C.D. Spies, Acetylcholinesterase inhibitors reduce neuro-inflammation and-degeneration in the cortex and hippocampus of a surgery stress rat model, PLoS One 8 (2013), e62679.
[35] S. Mostert, W. Mentz, A. Petzer, J.J. Bergh, J.P. Petzer, Inhibition of monoamine oxidase by 8-[(phenylethyl) sulfanyl] caffeine analogues, Bioorg. Med. Chem. 20 (2012) 7040–7050.
[36] C. Minders, J.P. Petzer, A. Petzer, A.C. Lourens, Monoamine oxidase inhibitory activities of heterocyclic chalcones, Bioorg. Med. Chem. Lett 25 (2015) 5270–5276.
[37] J. Yan, J. Hu, A. Liu, L. He, X. Li, H. Wei, Design, synthesis, and evaluation of multitarget-directed ligands against Alzheimer's disease based on the fusion of donepezil and curcumin, Bioorg. Med. Chem. 25 (2017) 2946–2955.
[38] B. Kumar, P. Sharma, V.P. Gupta, M. Khullar, S. Singh, N. Dogra, V. Kumar, Synthesis and biological evaluation of pyrimidine bridged combretastatin derivatives as potential anticancer agents and mechanistic studies, Bioorg. Chem. 78 (2018) 130–140.
[39] R.A. Friesner, J.L. Banks, R.B. Murphy, T.A. Halgren, J.J. Klicic, D.T. Mainz, M.P. Repasky, E.H. Knoll, M. Shelley, J.K. Perry, Glide: a new approach for rapid, accurate docking and scoring. 1. Method and assessment of docking accuracy, J. Med. Chem. 47 (2004) 1739–1749.
[40] L. Schrödinger, QikProp, Version 3.5, New York, NY, 2012.
[41] S. Release, 1: Desmond Molecular Dynamics System, Version 3.7, DE Shaw Research, New York, NY, Maestro-Desmond Interoperability Tools, Version 3, 2014.